

EmRad: Ubiquitous Vital Sign Sensing Using Compact Continuous-Wave Radars

Nils C. Albrecht ¹, Graduate Student Member, IEEE, Dominik Langer ², Graduate Student Member, IEEE, Daniel Krauss ³, Graduate Student Member, IEEE, Robert Richer ⁴, Luca Abel ⁵, Bjoern M. Eskofier ⁶, Senior Member, IEEE, Nicolas Rohleder ⁷, and Alexander Koelpin ⁸, Senior Member, IEEE

Abstract—In biomedical monitoring, non-intrusive and continuous tracking of vital signs is a crucial yet challenging objective. Although accurate, traditional methods, such as electrocardiography (ECG) and photoplethysmography (PPG), necessitate direct contact with the patient, posing limitations for long-term and unobtrusive monitoring. To address this challenge, we introduce the EmRad system, an innovative solution harnessing the capabilities of continuous-wave (CW) radar technology for the contactless detection of vital signs, including heart rate and respiratory rate. EmRad discerns itself by emphasizing miniaturization, performance, scalability, and its ability to generate large-scale datasets in various environments. This article explains the system's design, focusing on signal processing strategies and motion artifact reduction to ensure precise vital sign extraction. The EmRad system's versatility is showcased through various case studies, highlighting its potential to transform vital sign monitoring in research and clinical contexts.

Index Terms—Biomedical monitoring, doppler radar, machine learning.

Impact Statement— This publication introduces a novel millimeter-wave technology-based radar system, emphasizing usability for non-invasive vital sign monitoring, employing an LSTM classifier for precise individual heartbeat prediction.

Manuscript received 10 January 2024; revised 11 April 2024 and 22 May 2024; accepted 22 May 2024. Date of publication 28 June 2024; date of current version 15 August 2024. This work was supported by the Deutsche Forschungsgemeinschaft (DFG, German Research Foundation) – SFB 1483 – Project-ID 442419336, EmpkinS. The review of this article was arranged by Editor Paolo Bonato. (*Corresponding author: Nils C. Albrecht.*)

Nils C. Albrecht, Dominik Langer, and Alexander Koelpin are with the Institute of High-Frequency Technology, Technische Universität Hamburg, 21073 Hamburg, Germany (e-mail: nils.albrecht@tuhh.de).

Daniel Krauss, Robert Richer, and Luca Abel are with the Machine Learning and Data Analytics Lab, Friedrich-Alexander-Universität Erlangen-Nürnberg (FAU), 91054 Erlangen, Germany.

Bjoern M. Eskofier is with the Machine Learning and Data Analytics Laboratory, Friedrich-Alexander-Universität Erlangen-Nürnberg (FAU), 91054 Erlangen, Germany, and also with the Translational Digital Health Group, Institute of AI for Health, Helmholtz Zentrum München – German Research Center for Environmental Health, 85764 Neuherberg, Germany.

Nicolas Rohleder is with the Chair of Health Psychology, Institute of Psychology, Friedrich-Alexander-Universität Erlangen-Nürnberg (FAU), 91054 Erlangen, Germany.

Digital Object Identifier 10.1109/OJEMB.2024.3420241

I. INTRODUCTION

MEASURING human vital signs is a common task in all medical environments. It is well known that vital signs provide an excellent first approximation of a person's general state of health. Historically, human cardiac vital signs were measured using traditional, contact-based measurements such as electrocardiography (ECG) or photoplethysmography (PPG). These well-established methods deliver proven accuracy and are considered the gold standard for vital sign assessment, but require direct body contact. For many applications, this is undesirable, and contactless alternatives are beneficial.

Radar technology can capture vital signs by detecting minor changes in the distance between its antenna and the human body due to heart and respiratory activities [1]. During respiration, inhalation causes the lungs and chest to expand, decreasing this distance, while exhalation contracts them, increasing it. These changes, several millimeters in amplitude, are detectable even by basic radar systems. However, detecting heart activity is more challenging. Radar cannot measure electrophysiological heart activity like an ECG does. Instead, it can detect mechanical changes due to cardiac activity, like pulse waves, which arise from heart contractions pushing blood into arteries [2]. These cause minor expansions in blood vessels, slightly altering the distance to the radar, typically by several hundred micrometers. In addition, cardiac activity causes heart sounds that arise from the closure of the heart valves after blood ejection into the body. Like pulse waves, heart sounds induce measurable mechanical vibrations on the skin, which can be detected by radar. While their amplitude is considerably smaller (1 μm to 15 μm) [3], their distinct frequency characteristics help to differentiate them from respiratory signals.

Previous work has demonstrated that these vital signs can be measured using radar-based sensors. However, most are very complex, expensive, and bulky, hindering practical applications [4], [5], [6]. Moreover, these systems predominantly serve resting individuals, overlooking scenarios with elevated heart rates. Since radar-based vital sign sensing relies only on the distance between the body surface and the radar antenna, random body movements that are orders of magnitude larger in amplitude than the vital signs pose a considerable source of artifacts. In order to enable radar-based vital sign sensing

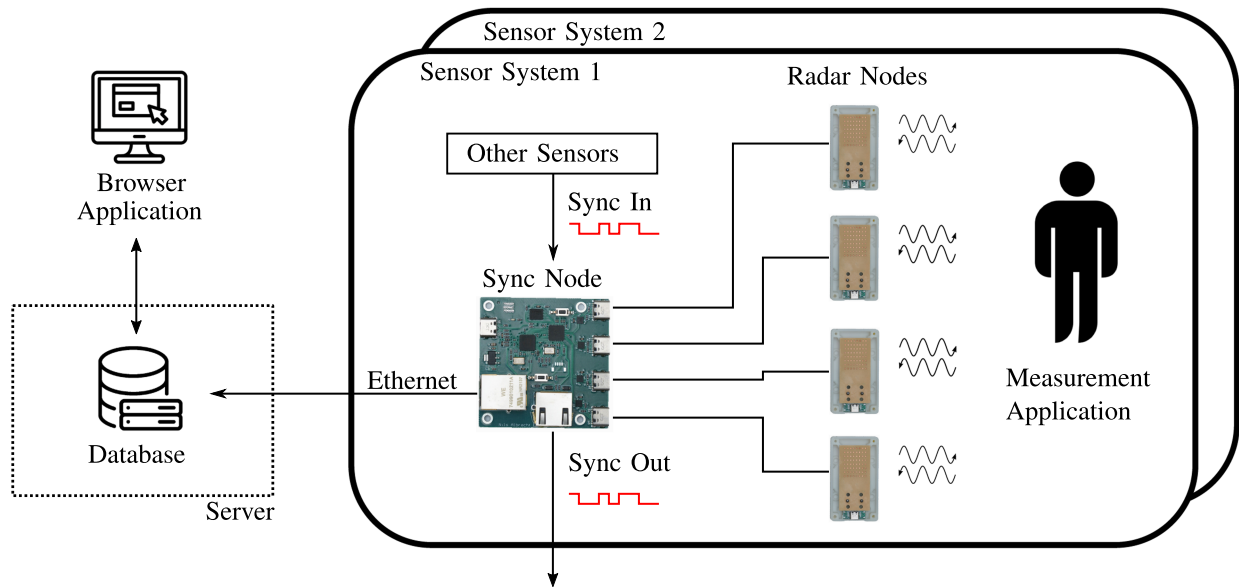


Fig. 1. System description of the *EmRad* system. Each sensor system contains up to four radar nodes as well as a sync node. Multiple deployed systems can be connected to a central database.

to be employed in different biomedical monitoring scenarios, there is a need to develop new solutions that allow a robust measurement of vital signs, even under the influence of large body movements [7].

In this publication, we present the radar-based sensor system *EmRad*, striving to solve these problems and enabling robust, vital sign sensing in various scenarios. Our system is designed to deliver high-quality data while being scalable for large deployments. Generating large datasets is crucial in the evolving landscape of machine-learning techniques in medical applications. Currently, no other system can generate these datasets at scale. The purpose of our research is, therefore, to present a system that addresses these shortcomings. This will enable us to effectively employ machine learning techniques and better understand the effects of large body movements.

In this paper, we summarize important design considerations and algorithmic choices. In addition, we showcase examples of different research projects in medicine and psychology that use the *EmRad* system to measure cardiopulmonary vital signs in various application scenarios.

II. MATERIALS AND METHODS

A. System Design

The basic principle of the *EmRad* system is depicted in Fig. 1. It consists of multiple sensor nodes which are connected to a synchronization node that collects data from up to four sensor nodes and transmits the measured data to a computer via Ethernet. In addition, the synchronization node allows the synchronization of other sensor devices (other *EmRad* nodes as well as external reference sensors), either by providing a synchronization as an output channel that is sampled by other sensor devices or by receiving an external synchronization signal via the input channel. This modular design allows the setup of various measurement scenarios and the integration of almost all

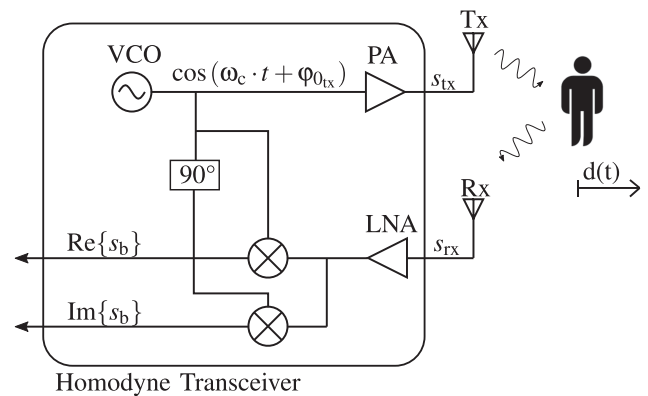


Fig. 2. Block diagram of the homodyne transceiver used for the radar system. The complex baseband signal is the main output used for further processing.

external reference sensors. This is especially important in a research context, as many interdisciplinary research undertakings rely on precise synchronization of different sensor modalities. Achieving this synchronization is often challenging, particularly when using commercial sensors. All hardware is enclosed in 3D-printed sealed enclosures, facilitating easy use.

The suggested radar system follows the unmodulated continuous wave (CW) radar design whose technical feasibility was already demonstrated in various publications [8], [9], [10]. This straightforward approach offers considerable benefits for detecting vital signs. The unmodulated carrier signal ensures that the system bandwidth is low, which introduces a minimal amount of noise. This comprises the main advantage of a CW radar: its high sensitivity. Even with minimal hardware, it can detect micrometer-scale movements [11]. The system design is illustrated in Fig. 2. A local oscillator produces a sinusoidal carrier, which is then amplified by a power amplifier and broadcast using an antenna. The reflected signal from the target is received and

down-converted to a complex baseband signal using a quadrature receiver setup. Finally, this complex, low-frequency signal is digitized using analog-to-digital converters (ADC).

The transmitted carrier with a carrier frequency $\omega_c = 2\pi f_c$ and zero phase $\varphi_{0_{tx}}$ can be denoted as:

$$s_{tx}(t) = A_{tx} \cdot \cos(\omega_c \cdot t + \varphi_{0_{tx}}). \quad (1)$$

The backscattered received signal s_{rx} is modeled as a time-delayed version of the transmit signal with an additional phase offset φ_{rx} and reduced amplitude A_{rx} :

$$s_{rx}(t) = A_{rx} \cdot \cos(\omega_c \cdot (t - \tau) + \varphi_{0_{tx}} + \varphi_{rx}). \quad (2)$$

By quadrature mixing this signal with the original transmit signal s_{tx} , a complex baseband signal $s_b(t)$ is obtained. The amplitude of this baseband signal is directly proportional to the reflected target power, while the phase argument

$$\begin{aligned} \varphi_b(t) &= \arg\{s_b(t)\} \\ &= \omega_c \cdot \tau - \varphi_{rx}, \end{aligned} \quad (3)$$

is directly proportional to the time delay τ . This time delay is a direct result of the propagation time of the electromagnetic wave towards the target at a distance of d and back to the receiver. It can, therefore, be calculated as:

$$\tau = \frac{2d}{c}. \quad (4)$$

Therefore, the target distance d can be derived from the received baseband signal $s_b(t)$. However, due to the ambiguity of the phase $\varphi_b(t)$ in 2π and the unknown phase offset φ_{rx} , it is not possible to directly calculate an absolute distance. However, displacement relative to a starting distance can be derived by employing phase unwrapping. As such distance changes between radar and the human body surface can, amongst others, originate from physiological processes, such as respiration, pulse wave propagation, or heart sounds, they can be used to predict vital signs.

In Fig. 4, we present the assembled circuit board of the proposed *EmRad* radar node without a mounted antenna. All the active radio frequency (RF) circuitry is contained within a commercially available monolithic microwave integrated circuit (MMIC) transceiver (*BGT60LTR11AIP*, Infineon, Neubiberg, Germany). While this MMIC was initially designed for cost-effective motion detectors, it houses a comprehensive homodyne transceiver operating in the 61 GHz Industrial, Scientific, and Medical (ISM) band [12]. We harness the in-built phase-locked loop (PLL) stabilized oscillator, low noise amplifier, and quadrature mixer while omitting the integrated baseband components. The transmit and receive signals are radiated directly from the MMIC package with integrated patch antennas on the surface. This simplifies hardware design, as no high-frequency signals are present on the circuit board. However, the integrated antennas feature very low gain and are therefore unsuitable for vital sign detection. In Section II-B, we present an innovative transition to connect to the integrated antennas and utilize a high-gain antenna to accurately detect vital signs.

The analog baseband signals of the transceiver are low-pass filtered with a cutoff frequency of 1000 Hz and subsequently sampled by a dual-channel simultaneous sampling ADC (*ADS131M02*, Texas Instruments, Dallas, TX, USA). Operating at a sampling frequency of 2000 Hz, the ADC exhibits a dynamic range of 106 dB, surpassing that of the frontend. This ensures that the system noise contribution of the ADC is negligible. Afterward, we digitize the signal at 24-bit resolution, translating to a data flow rate of 12 kB/s. Finally, we encode the samples using a constant overhead byte stuffing scheme on a microcontroller (*RP2040*, Raspberry Pi Foundation, Cambridge, U.K.) before sending them to the sync node. Although we leverage a commercially available Universal Serial Bus (USB) 2.0 physical layer for data transfer, our system incorporates a proprietary 1 Mbit/s protocol, which offers good robustness and also supports cable extensions of up to 10 m. All components are laid out on a single four-layer FR4 PCB that can easily be manufactured using an industry-standard process. Fig. 3 displays a cross-sectional view of one radar node with the circuit board on the bottom and an additional antenna stack on Top. As shown in Fig. 1, each radar node transmits its digitized baseband data toward the synchronization node for further processing. This way, the hardware of each radar node can be fairly simple, as no additional memory or real-time processing capability is needed. The synchronization node collects data from up to four sensor nodes and is connected to a computer or central server via Ethernet. Therefore, no special hardware or drivers are needed on the host side, and standard Ethernet switches can connect any number of nodes to a server.

B. Antenna Design

Single-channel continuous wave (CW) radar systems lack inherent lateral resolution and thus cannot differentiate between multiple targets. In contrast to multiple-input multiple-output (MIMO) based systems, a directional antenna is required to focus on a point of interest. Due to the difference in permittivity between air and the human body, some of the power transmitted to the upper body is reflected. To optimize system gain, the receive (*Rx*) and transmit (*Tx*) antennas must have the same field of view. Additionally, the spot projected on the chest should be small, with side lobes suppressed and grating lobes avoided to exclude any background movements.

In the context of developing a fully integrated radar transceiver, we focused on antenna optimization since it is the only optimizable component in the RF path. Since the *BGT60LTR11AIP* package lacks dedicated RF outputs and inputs for *Tx* and *Rx* signals, we were required to use the included antenna in package (AiP), which has limited capabilities. According to the datasheet, the AiP has a gain of 6 dBi, making it impractical for detecting vital signs. We opted for PCB technology to manufacture the antenna upgrade to ensure the system is scaleable and adaptable.

It is necessary to couple the power from the AiP into an intermediate structure that serves as an adapter between the AiP and a highly directive antenna on a PCB (Fig. 3). We situated an air-filled rectangular waveguide (RWG) ④ above the patch

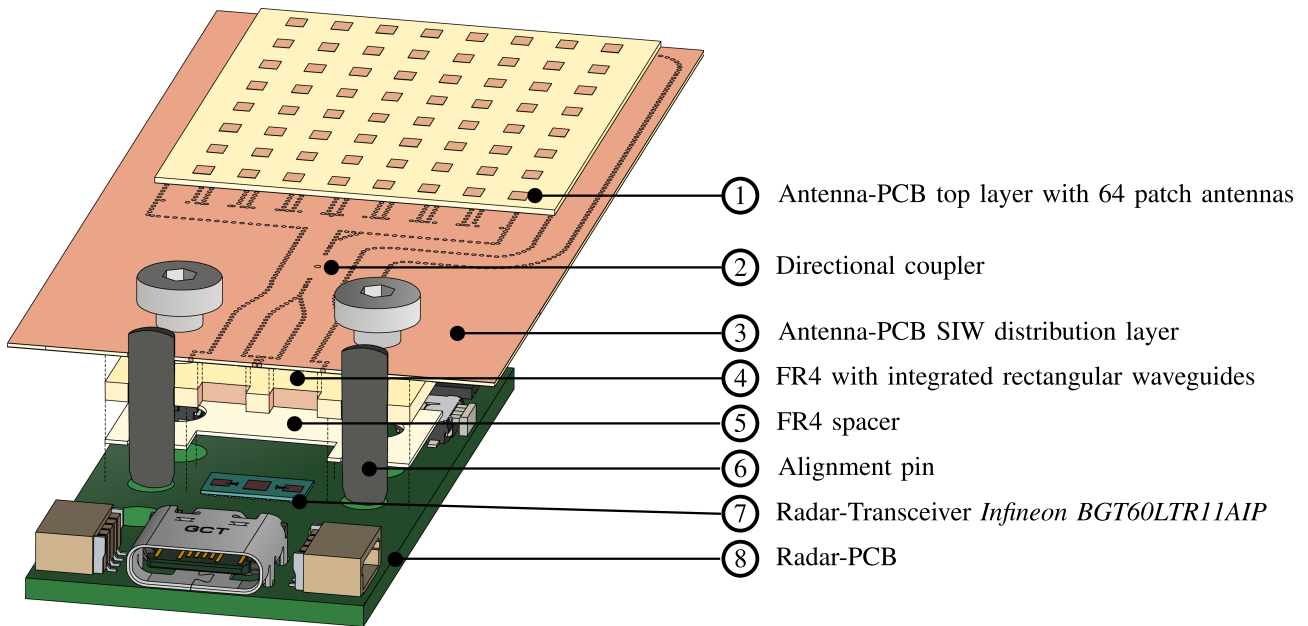


Fig. 3. Proposed radar system shown in exploded oblique projection. For clarity, the transition between the radar transceiver and antenna printed circuit board (PCB) is shown as a cross-section.

antennas of the transceiver ⑦. The RWG is a universal interface to which we can connect various antennas. We used an array of 8x8 slot-fed patch antennas ① with a substrate-integrated waveguide (SIW) distribution network ③, comparable to the antenna shown in [13]. We converted the bistatic antenna configuration of the transceiver chip to monostatic, employing a two-hole directional coupler ② in SIW technology, and assembled the antenna system by stacking the RWG adapter and the PCB antenna on Top of the MMIC package. The parts were aligned by two alignment pins ⑥ and held in place by screws. To prevent too much pressure being exerted on the transceiver by tightening the screws, we manufactured a spacer ⑤.

In simulation experiments, the upgraded antenna exhibited a gain of 23 dBi and a half-power beam width of 11° (Fig. 5), representing a considerable improvement compared to the AiP.

C. Sensitivity Evaluation

As the detection of heart sounds requires accurately discerning the timing of each heartbeat, it is crucial that the *EmRad* system can even detect the slightest movements with a high signal-to-noise ratio (SNR). One approach to ensuring this capability is to assess the received power from a human target and compare it to the noise power within the received baseband signal. However, there are several obstacles that prevents this method. First of all, the manufacturer of the radar transceiver did not provide crucial values such as the receiver conversion gain, the noise figure, or the transmitter output power. Furthermore, since the transceiver Integrated Circuit (IC) is permanently bonded to the Antenna in Package (AiP), obtaining these values through measurement is impractical.

Given the specific nature of our measurement application, traditional methods like the radar equation aren't applicable.

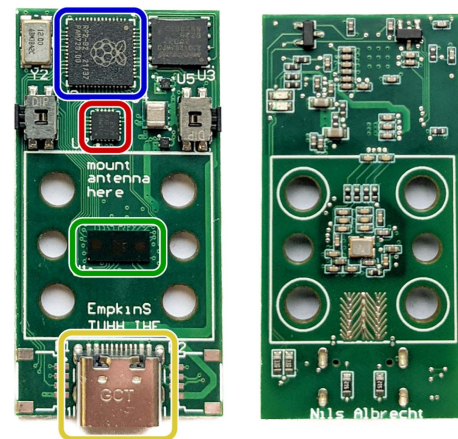


Fig. 4. Top and bottom view of the assembled circuit board of a *EmRad* radar node. The core components are highlighted: (—) *RP2040*, Raspberry Pi Foundation, Cambridge, U.K. (—) *ADS131M02*, Texas Instruments, Dallas, TX, USA (—) *BGT60LTR11AIP*, Infineon, Neubiberg, Germany (—) USB data connector.

The close proximity to the target prohibits does not allow to treat it as a single point; instead, it's distributed. Additionally, the receive antenna operates in the target's near field, rendering the concept of radar cross-section invalid.

For the *EmRad* system, our solution was to validate the system's sensitivity in the context of the application using a linear test bench. The measurement setup, depicted in Fig. 6, involves mounting an *EmRad* system in front of a single-axis linear test bench (*A 123*, *Physik Instrumente*, Auburn, MA, USA) with a copper disk serving as the target. Equipped with air bearings and a positioning system boasting positional repeatability of 100 nm, the test bench moves the target periodically at a frequency of 1 Hz, with amplitudes of $A_1 = 10 \mu\text{m}$ and $A_2 = 1 \mu\text{m}$, all while

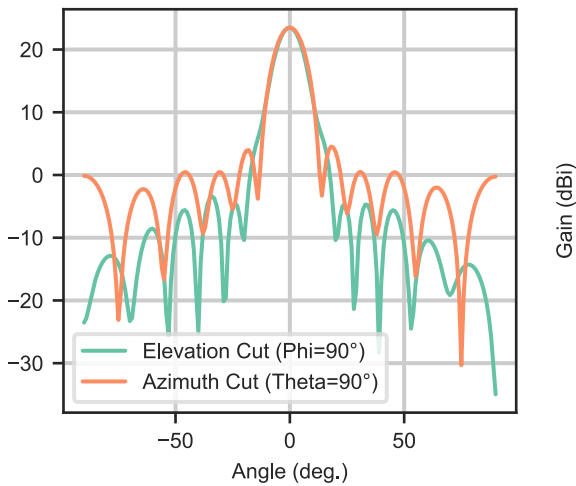


Fig. 5. Cuts of the simulated antenna radiation pattern in elevation and azimuth.

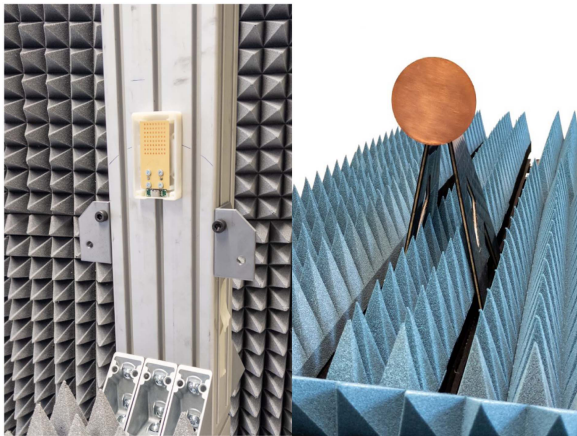


Fig. 6. Test setup for sensitivity evaluation. The *EmRad* radar node is mounted to a test fixture (left) and illuminates a copper target disk $D = 80$ mm on a precision linear stage (right).

recording the radar baseband signals. The amplitudes of heart sounds are between $1 \mu\text{m}$ and $15 \mu\text{m}$ [3], therefore the chosen amplitudes define the minimum resolution to detect those. We opted for a target diameter of $D = 80$ mm at a distance of 1 m, a configuration roughly resembling the size of the area from which heart sounds emanate in our application.

D. Processing Pipeline

One synchronization node of the *EmRad* system can connect up to four sensor nodes for synchronization and data transfer. The synchronization node features an Ethernet connection for data transfer to a central host. The baseband data from the radar nodes are packetized into standard User Datagram Protocol (UDP) packets and subsequently transferred to the host. Each sensor possesses a unique identifier, ensuring every network packet is tagged accordingly and packet counters are incorporated into the datagrams. For each sensor node, the incoming and outgoing synchronization signal is carried in parallel with the complex baseband data stream. In larger deployments, like

hospitals with numerous patient beds, multiple masters can link to a singular backend server. This server, built on *NodeJS*, instantly logs incoming packets into a provisional database with receive timestamps, guaranteeing the tracking of all sensor data upon network connection.

In the web-based frontend software, users can create measurement series using sensor data and specify start time, end time, sensor nodes, and additional metadata. After the end of the measurement, an automatic export job consolidates data from the selected nodes into a single file through several steps:

- *Packet Selection*: Identification and retrieval of UDP packets with correct timestamps and node IDs from the local database.
- *Packet Reordering*: Due to potential sequence disruptions from network or operating system latencies, packets are reordered using counters; missing packets are substituted with zero-valued dummy packets.
- *Packet parsing*: Network packets are processed to extract samples and synchronization signals; afterward, all node data from one measurement is stored in a labeled, structured *HDF5* file.

The resulting *HDF5* file compiles samples from all nodes, but extended recording times cause synchronization issues due to clock inaccuracies and varying sampling rates across nodes and reference sensors. The synchronization signal from all devices is transformed to the frequency domain. The actual sampling rate from each sensor is derived from this synchronization signal, assuming a precise source clock. Resampling aligns all sensors to a consistent rate, and cross-correlation on the synchronization signals ensures a unified starting point, yielding a fully synchronized dataset from all nodes.

E. Machine Learning-Based Processing

To mitigate the challenges introduced by large body movements, which made direct phase demodulation difficult, we employ machine learning (ML) for data extraction. Specifically, we use a bidirectional long short-term memory (LSTM) architecture as demonstrated in [14], [15], [16]. We constructed a set of vectors derived from the radar's complex baseband signals that serve as input to the LSTM network:

- The magnitude and argument of the in-phase- and quadrature-signals, after high-pass filtering using a (using a fourth-order Butterworth filter with a cutoff frequency of 0.1 Hz),
- The magnitude of I- and Q-signals after band-pass filtering using a fourth-order Butterworth filter with a frequency range of 18 Hz to 80 Hz, subsequently transformed using the Hilbert envelope,
- I- and Q-signals after low-pass filtering using a fourth-order Butterworth filter with a 10 Hz cutoff.

These vectors are downsampled to a 100 Hz sampling frequency, as higher bandwidth components are no longer present. The resampled vectors are then introduced into our LSTM model, consisting of two layers, each with 256 LSTM cells (Fig. 7). The completion of this neural network is a single-output fully connected layer.

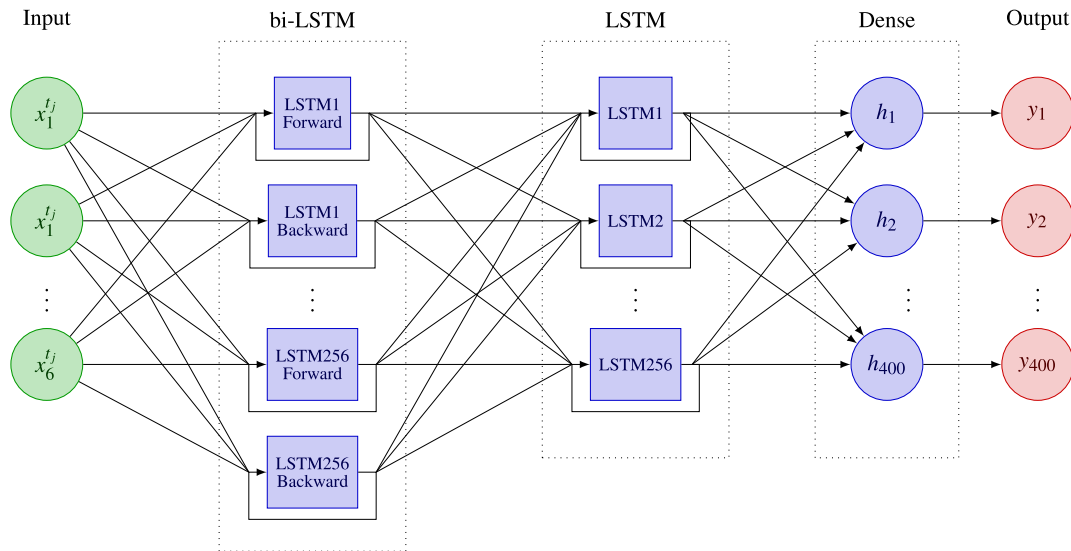


Fig. 7. Network graph of the proposed heartbeat detection network. The input is a $\{400 \times 6\}$ tensor with 400 time steps and six variables. The output is a single vector with 400 time steps.

The LSTM architecture was first presented by Hochreiter et al. [17] and is commonly used for time series data. It is a Recurrent Neural Network (RNN) type and can thus model long-term dependencies of input data. Each unit employs an input, forget, and output gate to cope with problems with other traditional RNN schemes. Mathematical derivation of the LSTM unit cell is available in the original publication [17]. Effectively, we use the model to perform sequence-to-sequence classification with the input being a tensor of 6 input variables and 400 samples length and the output tensor being a single variable with 400 samples length. The first LSTM layer is used as a bidirectional layer, as input sequences are fed separately into the respective sections in forward and backward directions, thus effectively doubling the layer. Outputs for the forward and backward branches are concatenated to form a larger tensor. The first LSTM layer is configured to output a full tensor for every input sample, resulting in an output shape of 400×512 . The second LSTM layer uses only forward processing, and only the output after the last time step is captured, so the resulting output shape is a tensor of size 512. The final fully connected layer is used to produce an output of 400 samples.

For model training, we created a dataset of synchronized radar and ECG recordings of 23 individuals lying at rest with a total recording duration of 100 h. We segmented heartbeats based on R-peaks extracted from the ECG using the Pan-Tompkins algorithm [18]. We chose not to use binary R-peak labels to improve the model's training accuracy and convergence, which can present difficulties as they are not continuously differentiable in time. Instead, we smoothed the R-peak signals using a Gaussian kernel with a spread of 10 ms. This method changes the abrupt binary labels into a continuous series of Gaussian-shaped pulses, making the data more model-friendly. Each pulse in this vector indicates the R-peak occurrence probability at its corresponding timestamp.

We trained the model using the *Adam* optimizer [19] with a learning rate of 0.01 and used data segments with a length of 4 s

and an overlap of 3.5 s as model input. The loss is evaluated using a mean-square error function. The final output of the LSTM model is interpreted as R-peak probability, as the training labels are constructed as such. Consequently, we applied a peak detection algorithm on the output to identify the heartbeat locations during inference using the `find_peaks` from the *scipy* package with an experimentally derived amplitude threshold of 0.5.

During inference, the input samples are fed in 300 sample overlapping windows, and only the centermost 100 samples are considered as output. This effectively mitigates edge effects and ensures at least one heartbeat before and after the evaluation window is present in the input data.

In addition to the heartbeats, we extracted the breathing rate from the baseband data. Unfortunately, as breathing can be controlled voluntarily, no valid assumptions can be made regarding periodicity. Therefore, band-pass filtering, as commonly proposed, does not usually deliver meaningful results. Instead, we directly calculate the distance using *arctan* demodulation with subsequent unwrapping. We employ a least squares circle fitting with a Kalman filter to track the offsets to remove the constant offsets in the signal before calculating the argument. The resulting distance is band-pass filtered with a pass band of 0.05 Hz to 0.5 Hz using a fourth-order Butterworth filter. The breathing rate is calculated using a peak search. Since this approach for breathing rate estimation can not distinguish between breathing and random movements, it can only be applied when individuals directly face the antenna, and the amount of random large body movements is reduced to a minimum.

F. Feasibility Experiments

After training, we deployed the machine learning to various research projects to examine the feasibility of using contactless heart rate assessment in various data collection scenarios. In the following section, we present three different deployment

use cases. All studies were approved by the Ethics Commission of FAU Erlangen-Nürnberg under protocol numbers 20-486_1-B and 493_20-B.

1) Instantaneous Heart Rate: In this use case, we demonstrated the general feasibility of the *EmRad* system. We measured the cardiac activity of $n = 4$ participants sitting at rest in front of the *EmRad* system while synchronously recording a 1-channel ECG (*Biopac MP36*, Biopac, Goleta, CA, USA) as reference. Afterwards, we applied our proposed processing pipeline to extract individual heartbeats and respiration from the recorded baseband data. We directly compared the interbeat intervals between radar and ECG reference for this use case.

2) Longitudinal Sleep Monitoring: Radar-based vital sign monitoring has the potential to facilitate longitudinal sleep monitoring, which traditionally relies on collecting multimodal physiological data in an unfamiliar laboratory environment using obtrusive polysomnography (PSG) systems.

In this use case, we used data from an overnight sleep study of $n = 44$ participants, resulting in a total of 239.6 h of sleep data. We placed four radar nodes as a horizontal array below the mattress of a hospital bed and used synchronized ECG recordings from a polysomnography system (*Somno HD*, *Somnomedics*, *Randesacker*, Germany). Thereby, the signals of those radar nodes were sent to a master node that combined the datastreams of the single radar nodes and triggered an m-sequence signal for synchronization. We extracted heart sounds from each radar node individually using our proposed pipeline and fused the output of the four radar nodes by selecting the sensor with the highest confidence for detected heartbeats for every 30-second window. Subsequently, we used the predicted heartbeats to calculate the mean heart rate, which we then compared with the heart rate obtained from the ECG. Within this process, we smoothed the heart rate extracted from the radar signal using a 10-point moving average filter and interpolated missing values by linear interpolation.

3) Acute Psychosocial Stress Assessment: In stress research, heart rate (variability) (HR(V)) is a common measure to assess the activity of the autonomic nervous system (ANS) [20]. Traditionally, HR(V) is computed using data from contact-based modalities, such as ECG. While this procedure is considered unobtrusive, it can still interfere with human behavior during psychological studies [21]. Radar-based methods have the potential to allow a more unobtrusive and realistic observation of human behavior, particularly ANS activity, during stress.

To assess the feasibility of using the proposed system in this context, we acquired data from $n = 23$ participants during a study using the Trier Social Stress Test (TSST) [22], the gold standard for acute stress induction in the laboratory. It consists of a public speaking task in the form of a fictional job interview, followed by a mental arithmetic task. Both tasks are performed in front of a two-person panel who are trained to remain completely neutral, show as little emotion as possible, and not engage in any interaction throughout the whole procedure [23]. While the original TSST protocol required participants to stand in front of the panel, we modified the protocol and asked participants to remain seated throughout the entire TSST to minimize the effect of random large-body movements.

We placed one radar sensor in front of the participant using a tripod. The sensor height was adjusted for each participant, with the antenna being directed towards the chest of the individual 10 cm below the jugular notch, as shown in Fig. 9. Concurrently, we collected ECG recordings using a *Biopac MP160* (Biopac, Goleta, CA, USA) system. Both systems were synchronized using an external synchronization peak, which was sampled as an analog signal from both the *Biopac* and the *EmRad* system.

Using our proposed pipeline, we estimated heartbeats from radar data and performed a beat-to-beat comparison to the reference ECG. In addition, we computed the Pearson correlation to assess the relationship between the heart rate derived from the ECG and the radar sensor data.

III. RESULTS

A. Sensitivity Evaluation

Using the proposed test setup, we recorded the system response for target movements from $10 \mu\text{m}$ down to $1 \mu\text{m}$. Fig. 10 presents the phase of the recorded baseband signals for a time of 4 s. The signals are unfiltered and shown with a bandwidth of 500 Hz. The target was moved in a rectangular function with a frequency of 1 Hz, with amplitudes of $A_1 = 10 \mu\text{m}$ and $A_2 = 1 \mu\text{m}$. According to (3), this corresponds to received phase deviations of $\Delta\Phi_1 = 1.5^\circ$ and $\Delta\Phi_2 = 0.15^\circ$ respectively. It is visible that the system can resolve the rectangular shape of the waveform exceptionally well and even the tiny movement amplitude is not buried in noise despite the high measurement bandwidth. This proves the radar system's outstanding sensitivity and noise performance, enabling it to capture tiny surface vibrations, such as heart sounds. Slight signal drift due to thermal effects is visible in both signals; however, due to its low-frequency content, it does not interfere with vital sign detection.

B. Instantaneous Heart Rate

Fig. 8 demonstrates the outcomes of our processing pipeline, applied to individuals in a resting seated position. The pipeline incorporates radar heart sounds as a key input feature for an LSTM network, effectively highlighting the periodic nature of cardiac activity. The certainty output from the LSTM demonstrates a strong correlation with synchronous reference ECG data. Our results show that the instantaneous heart rate exhibits high agreement between the two modalities. Modulation of the interbeat intervals due to the respiratory arrhythmia is clearly visible. Over a period of 60 s, the mean difference of the interbeat intervals measured by radar and ECG is 4 ms with a standard deviation of 61 ms.

C. Longitudinal Sleep Monitoring

The mean heart rate calculated in 30 s epochs of one selected participant over one entire night in the sleep laboratory is displayed in Fig. 11. Heart rate estimation was possible on the whole dataset with a mean absolute error (MAE) of 1.28 ± 2.12 bpm. The performance was consistent across right, left, supine, or prone sleep poses.

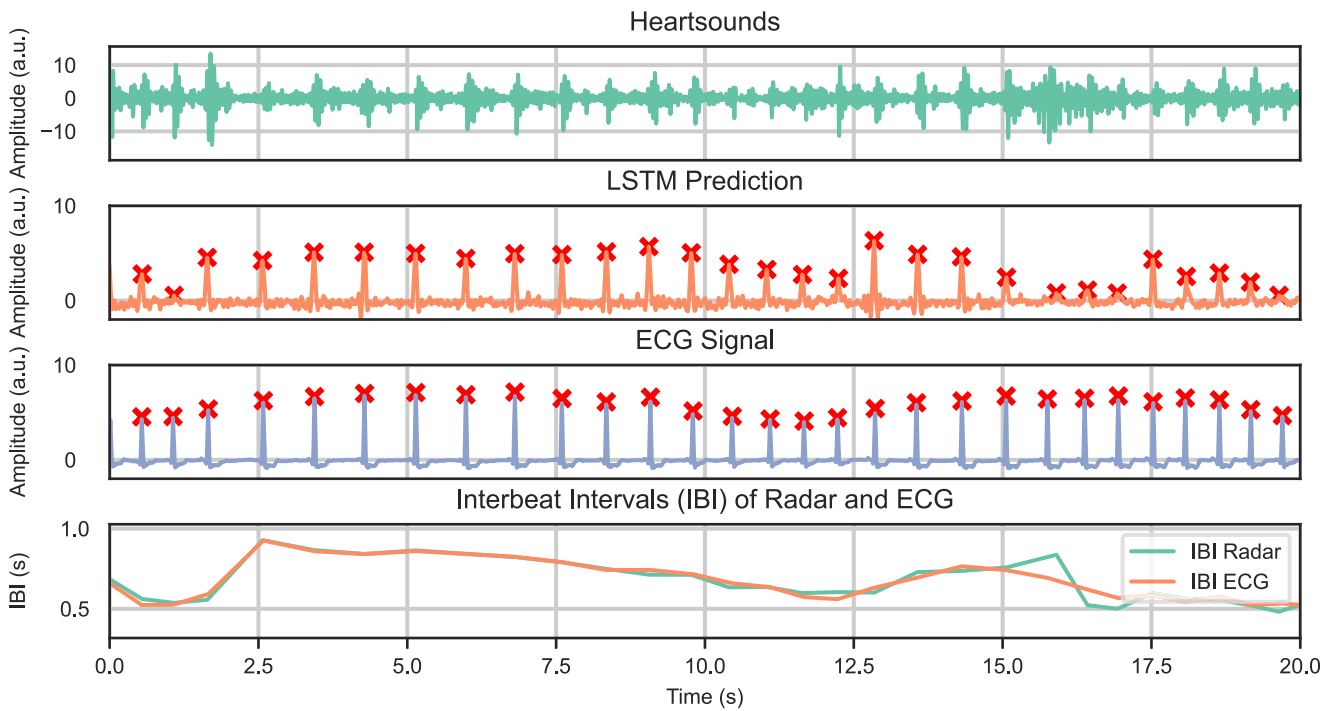


Fig. 8. Extracted heart sounds and LSTM prediction with respective reference ECG for a 20 s window of a sitting person. The interbeat intervals derived from the LSTM and ECG are displayed in an interpolated fashion.

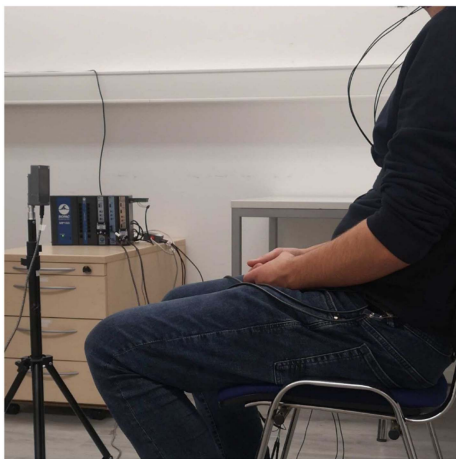


Fig. 9. Setup of the conducted stress study.

Thereby, the MAE per participant ranged from 0.39 ± 0.41 bpm to 5.99 ± 5.87 bpm which is potentially caused by a different positioning in bed, such as lying more towards the bottom of the bed, resulting in the position of the radar being further away from the chest.

Furthermore, we examined the influence of activity during the night, measured by an actigraph, on the heart sound extraction. We performed a Pearson correlation analysis on the MAE of the extracted heart rate and the activity counts from the actigraph and found small to medium correlations with $r = 0.27$.

This excellent contactless heart sound extraction opens up the possibility of deriving parameters like heart rate variability,

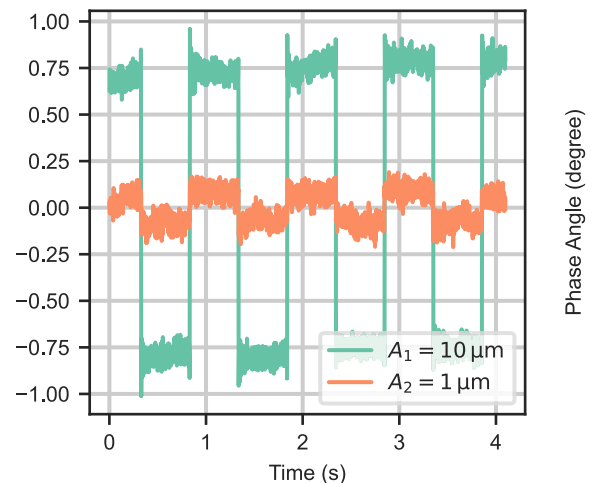


Fig. 10. Extracted baseband phase from rectangular movements of the synthetic target described in Section II-C.

enabling a deeper understanding of natural human sleep. Furthermore, it might serve as input for more sophisticated applications, such as sleep staging based on deep learning algorithms.

D. Acute Psychosocial Stress Assessment

Our proposed pipeline successfully identified heart rate trends during an acute stress test, supported by a strong Pearson correlation of 0.78 between heart rates obtained from both modalities. However, multiple heartbeats were not detected (Fig. 12). This is largely caused by motion artifacts due to random large body

TABLE I
COMPARISON OF THIS WORK WITH OTHER STATE-OF-THE-ART PUBLISHED CW RADAR SYSTEMS FOR VITAL SIGN DETECTION

	Frequency	Channels	Synchronization	Demonstrated Scenario	Signal Processing	Output
[24]	24 GHz	1	No	Sitting Still	FFT	Average Heart Rate
[25]	24 GHz	1	No	Sitting Still	Filter Bank	IBI's
[14]	24 GHz	1	Yes	Lying	LSTM	IBI's
[26]	120 GHz	1	No	Sitting Still	Filter Bank	Heart sounds
[27]	24 GHz	4	No	Lying	Filter Bank	Heart sounds
[28]	61 GHz	1	Yes	Lying	Filter Bank	Heart sounds
[29]	5.8 GHz	1	No	Sitting Still	FFT	Average Heart Rate
This Work	61 GHz	Unlimited	Yes	Lying, Sitting, Standing in different medical setups	LSTM	IBI's

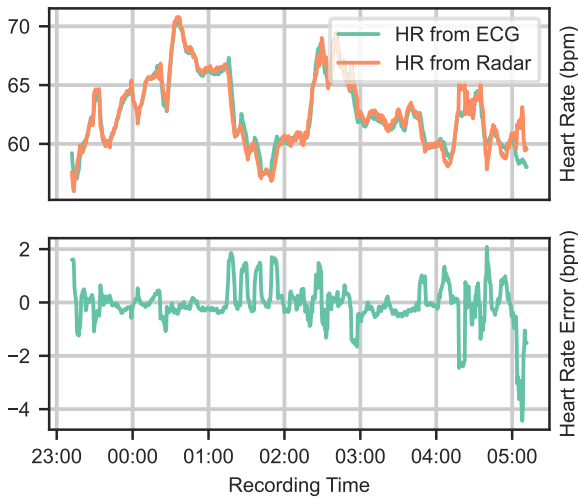


Fig. 11. Heart rates extracted from ECG and radar collected from one participant during an overnight sleep study (Top) and error between both modalities (bottom). HR outputs from ECG and radar were filtered with a 30 s moving average filter.

movements during the stress induction task. To assess the feasibility of the *EmRad* system in realistic research environments, we chose not to instruct participants to move as little as possible. Instead, they were asked to behave as naturally as possible during the TSST in order not to interfere with the stress protocol.

IV. DISCUSSION

Our findings suggest that our *EmRad* system yields promising results for non-invasive heart rate monitoring in stationary applications, demonstrating accurate interbeat interval estimation with only minor errors compared to an ECG reference. The heart rate trends correlated with sleep stages and nocturnal activities are detectable, demonstrating the effectiveness of the proposed system for this application. However, these measurements were collected in controlled environments, and we anticipate a need for adjustments in less predictable settings. Challenges arise in more active scenarios, such as during stress tests with participants moving and speaking, where our proposed approach currently struggles with accurate HR(V) estimation due to motion-related artifacts.

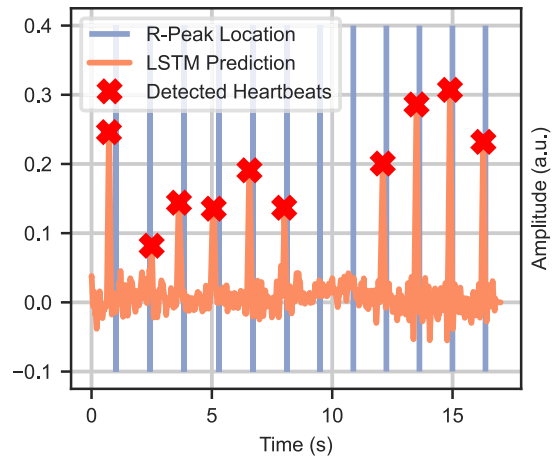


Fig. 12. Extracted heart sounds and LSTM prediction with reference R-peaks from ECG for a 20 s window of a participant during an acute stress test.

Yet, even under these conditions, the *EmRad* can still offer a heart rate reading. Future developments will focus on enhancing the ability of the system to monitor vital signs in the presence of large body movements. By collecting larger datasets tailored for ML-based vital sign extraction, we expect to improve the system's capability to function reliably across a broader range of activities.

Compared to other published systems, the *EmRad* system excels in the modularity and versatility of measurement applications. We show other CW systems with comparable specifications in Table I. Notably, *EmRad* is the only system designed to collect large-volume data with multiple channels and synchronized reference sensor recordings. In addition, our presented system is significantly more compact than all others, enabling ubiquitous measurements in diverse research contexts.

V. CONCLUSION

We presented the *EmRad* system, a 61 GHz radar system capable of detecting human vital signs in different scenarios. We achieve a small form factor with high measurement performance by combining a state-of-the-art transceiver circuit with a novel AiP to waveguide transition and a high-efficiency SIW antenna. Due to its small size and deep integration with application

software, it can be easily deployed to various settings while being interoperable with existing sensors. Alongside, we deployed an LSTM-based processing pipeline to extract individual heartbeats from the radar baseband data. The presented scenarios demonstrated commendable temporal precision performance compared to an ECG reference. However, large body movements still cause considerable artifacts that need to be addressed in future work. Thus, our objective is to enhance the resilience of the ML-based extraction pipeline, especially in demanding environments. We plan to leverage data aggregated from a network of *EmRad* sensors deployed across various research projects to further improve the performance and robustness of our *EmRad* system based on this large and diverse dataset.

CONFLICT OF INTEREST

The authors have no conflicts of interest to declare.

AUTHOR CONTRIBUTION

NCA was primarily responsible for designing the system and writing the paper. DL designed the antenna system and wrote the respective section of the paper. DK, RR, LA, BME, NR, and AK contributed their specialized expertise to their respective research domains and applications. All authors provided critical feedback and helped shape the research, analysis and manuscript.

ACKNOWLEDGMENT

We thank our colleague Bartosz Tegowski for his valuable expertise, which greatly assisted us in the writing of this paper.

REFERENCES

- [1] G. Paterniani et al., "Radar-based monitoring of vital signs: A tutorial overview," in *Proc. IEEE*, vol. 111, no. 3, pp. 277–317, Mar. 2023.
- [2] J. Alastruey et al., "Arterial pulse wave haemodynamics," in *Proc. 11th Int. Conf. Press. Surges*, 2012, pp. 401–443.
- [3] C. Will et al., "Radar-based heart sound detection," *Sci. Rep.*, vol. 8, no. 1, Dec. 2018, Art. no. 11551.
- [4] S. Schellenberger et al., "A dataset of clinically recorded radar vital signs with synchronised reference sensor signals," *Sci. Data*, vol. 7, no. 1, Dec. 2020, Art. no. 291.
- [5] T. Zhang, J. Sarrazin, G. Valerio, and D. Istrate, "Estimation of human body vital signs based on 60 GHz doppler radar using a bound-constrained optimization algorithm," *Sensors*, vol. 18, no. 7, Jul. 2018, Art. no. 2254.
- [6] A. Prat, S. Blanch, A. Aguasca, J. Romeu, and A. Broquetas, "Collimated beam FMCW radar for vital sign patient monitoring," *IEEE Trans. Antennas Propag.*, vol. 67, no. 8, pp. 5073–5080, Aug. 2019.
- [7] Q. Lv et al., "Doppler vital signs detection in the presence of large-scale random body movements," *IEEE Trans. Microw. Theory Techn.*, vol. 66, no. 9, pp. 4261–4270, Sep. 2018.
- [8] J. Salmi, O. Luukkonen, and V. Koivunen, "Continuous wave radar based vital sign estimation: Modeling and experiments," in *Proc. IEEE Radar Conf.*, 2012, pp. 0564–0569.
- [9] G. Vinci et al., "Six-port radar sensor for remote respiration rate and heartbeat vital-sign monitoring," *IEEE Trans. Microw. Theory Techn.*, vol. 61, no. 5, pp. 2093–2100, May 2013.
- [10] C. Li, V. M. Lubecke, O. Boric-Lubecke, and J. Lin, "A review on recent advances in doppler radar sensors for noncontact healthcare monitoring," *IEEE Trans. Microw. Theory Techn.*, vol. 61, no. 5, pp. 2046–2060, May 2013.
- [11] B. Scheiner, F. Michler, F. Lurz, R. Weigel, and A. Koelpin, "Nothing beats SNR: Single-digit micrometer ranging using a low-power CW radar featuring a low-weight 3D-Printed horn antenna," *IEEE Microw. Mag.*, vol. 21, no. 1, pp. 88–95, Jan. 2020.
- [12] "BGT60LTR11AIP, low power 60 GHz doppler radar sensor with antennas in package," Infineon, 2022.
- [13] T. Mikulasek, J. Lacik, J. Puskely, and Z. Raida, "Design of aperture-coupled microstrip patch antenna array fed by SIW for 60GHz band," *IET Microwaves, Antennas Propag.*, vol. 10, no. 3, pp. 288–292, Feb. 2016.
- [14] K. Shi et al., "Contactless analysis of heart rate variability during cold pressor test using radar interferometry and bidirectional LSTM networks," *Sci. Rep.*, vol. 11, no. 1, Dec. 2021, Art. no. 3025.
- [15] K. Shi et al., "Segmentation of radar-recorded heart sound signals using bidirectional LSTM networks," in *Proc. IEEE 41st Annu. Int. Conf. Eng. Med. Biol. Soc.*, 2019, pp. 6677–6680.
- [16] C. Ye, G. Gui, and T. Ohtsuki, "Deep clustering with LSTM for vital signs separation in contact-free heart rate estimation," in *Proc. IEEE Int. Conf. Commun.*, 2020, pp. 1–6.
- [17] S. Hochreiter and J. Schmidhuber, "Long short-term memory," *Neural Comput.*, vol. 9, no. 8, pp. 1735–1780, 1997. [Online]. Available: <https://doi.org/10.1162/neco.1997.9.8.1735>
- [18] J. Pan and W. J. Tompkins, "A real-time QRS detection algorithm," *IEEE Trans. Biomed. Eng.*, vol. BME-32, no. 3, pp. 230–236, Mar. 1985.
- [19] D. P. Kingma and J. Ba, "Adam: A method for stochastic optimization," *CoRR*, vol. abs/1412.6980, 2014.
- [20] S. Gradl, M. Wirth, R. Richer, N. Rohleder, and B. M. Eskofier, "An overview of the feasibility of permanent, real-time, unobtrusive stress measurement with current wearables," in *Proc. 13th EAI Int. Conf. Pervasive Comput. Technol. Healthcare*, 2019, pp. 360–365.
- [21] A. E. Kazdin, "Unobtrusive measures in behavioral assessment," *J. Appl. Behav. Anal.*, vol. 12, no. 4, 1979, Art. no. 1311490.
- [22] C. Kirschbaum, K.-M. Pirke, and D. H. Hellhammer, "The 'trier social stress test' a tool for investigating psychobiological stress responses in a laboratory setting," *Neuropsychobiology*, vol. 28, no. 1-2, pp. 76–81, 1993.
- [23] R. Richer et al., "Machine learning-based detection of acute psychosocial stress from body posture and movements," *Sci. Rep.*, vol. 14, no. 1, Apr. 2024, Art. no. 8251.
- [24] G. Vinci et al., "Six-port radar sensor for remote respiration rate and heartbeat vital-sign monitoring," *IEEE Trans. Microw. Theory Techn.*, vol. 61, no. 5, pp. 2093–2100, May 2013.
- [25] V. L. Petrović, M. M. Janković, A. V. Lupšić, V. R. Mihajlović, and J. S. Popović-Božović, "High-accuracy real-time monitoring of heart rate variability using 24 GHz continuous-wave doppler radar," *IEEE Access*, vol. 7, pp. 74721–74733, 2019.
- [26] L. Wen, S. Dong, C. Gu, and J.-F. Mao, "A compact non-contact heart sound sensor based on millimeter-wave radar," in *Proc. IEEE MTT-S Int. Microw. Biomed. Conf.*, 2022, pp. 305–307.
- [27] F. Michler et al., "A radar-based vital sign sensing system for in-bed monitoring in clinical applications," in *Proc. IEEE German Microw. Conf.*, 2020, pp. 188–191.
- [28] M. Wenzel, D. Langer, A. Koelpin, and F. Lurz, "A modular 61 GHz vital sign sensing radar system for long-term clinical studies," in *Proc. IEEE Topical Conf. Wireless Sensors Sensor Netw.*, 2024, pp. 18–21.
- [29] H. Jeong, D. Kim, G. Kim, and S. Kim, "VitRad: A low-cost continuous wave doppler radar system with 3D-printed horn antennas for human vital sign detection," *HardwareX*, vol. 12, 2022, Art. no. e00361.